Quantification of microbubble concentration through x-ray phase contrast imaging

T. P. Millard,[1, a)] M. Endrizzi,[1] L. Rigon,[2, 3] F. Arfelli,[2, 3] R. H. Menk,[4] J. Owen,[5] E. Stride,[5] and A. Olivo[1]
[1)] *Department of Medical Physics and Bioengineering, University College London, Malet Place, Gower Street, London WC1E 6BT, UK*
[2)] *Department of Physics, University of Trieste, Via Valerio 2, 34127 Trieste, Italy*
[3)] *Istituto Nazionale di Fisica Nucleare-Sezione di Trieste, Via Valerio 2, 34127 Trieste, Italy*
[4)] *Sincrotrone Trieste SCpA, S. S. 14km 163.5, 34012 Basovizza (TS), Italy*
[5)] *Institute of Biomedical Engineering, Old Road Campus Research Building, University of Oxford, Oxford OX3 7DQ, UK*

(Dated: 28 August 2013)

The use of microbubbles as a contrast agent for x-ray phase contrast imaging could both transform x-ray imaging into a 'functional' modality, and enable much needed monitoring of targeted drug delivery. To realize these benefits, it is essential to be able to quantify bubble concentration in a given tissue volume. We developed and validated a model that enables this to be achieved not only for phase-retrieved images obtained by processing multiple frames, but also on 'single-shot' images, a likely necessity in *in-vivo* implementations. Our experimental validation was based on analyzer-based imaging, but extension to other phase-based modalities is straightforward.

X-ray phase contrast imaging (XPCi) allows for imaging based on perturbations of the x-ray wavefront instead of absorption. This provides increased contrast, as terms governing wavefront deviation are typically a few orders of magnitude larger than that determining absorption. XPCi also provides extra information about a sample from the additional contrast mechanisms made available which, as well as refraction/interference,[1,2] include the dark field signal i.e. ultra-small-angle x-ray scattering (USAXS).[3–6]

Microbubbles have been investigated as a contrast agent for XPCi as they act as an x-ray lens, with individual microbubbles refracting and a population of microbubbles 'scattering' x-rays, as a consequence of multiple refraction in many directions.[7,8] This multiple scattering can thus be used to generate an area contrast leading to potential use of microbubbles as an XPCi contrast agent.

In comparison to conventional Iodine based contrast agents, microbubbles have been suggested to be safer,[8] and offer possibilities to develop novel imaging approaches as they generate contrast through an alternative physical mechanism, creating a signal that can be differentiated from absorption.

Preliminary evidence that microbubbles can be effectively used as contrast agent was obtained at synchrotrons using both analyzer based imaging (ABI)[8] and free space propagation,[9] and with a laboratory source using Talbot-Lau interferometry.[10] XPCi USAXS CT has already been performed, indicating that microbubbles could also be used in 3D forms of XPCi.[11]

The USAXS signal has previously been modeled for monodisperse microspheres and wires using wave optical and numerical approaches. No experimental verification has though been previously obtained for a model of microbubble USAXS signal from varying concentration of polydisperse microbubbles. As monodisperse microbubbles are difficult to fabricate, expensive, and therefore unlikely to be used in medical imaging, modelling the signal from polydisperse microbubbles (which are already commercially available) is of great importance for understanding the application of microbubbles to clinical XPCi.[12–15]

The work presented here demonstrates the use of a Monte Carlo based model for simulating polydisperse microbubbles in ABI, using both scatter retrieval and 'single-shot' methods. We have initially chosen to validate our model through ABI as it is well understood, allows scatter retrieval using three images, and has the potential for single-shot scatter based imaging. A single-shot method requires no crystal movement, as would probably be required by *in-vivo* applications, and any form of time-resolved imaging. While imaging at multiple rocking curve (RC) positions allows the extraction of scatter, apparent absorption and refraction images; a single-shot image on the RC tail produces an image based predominately on scatter. We demonstrate here that this can be used to measure changes in microbubble concentration. As such, this can be used for fast quantitative assessment of changes in polydisperse microbubble concentration, as would be found e.g. during microbubble disruption in targeted drug delivery with short pulses of targeted ultrasound.

A Monte Carlo model has previously been developed by some of the authors to model the USAXS signal from PMMA microspheres using ABI.[4] These microspheres

[a)] Electronic mail: t.millard@ucl.ac.uk

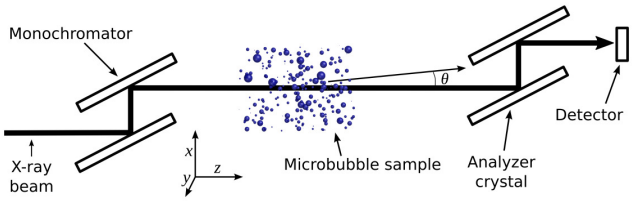

FIG. 1. Diagram depicting the passage of the undeviated x-ray beam through the imaging system, and a single photon refracted by the angle θ on the x-z plane.

were monodisperse, larger than clinical microbubbles, and more densely packed. Comparison between simulation and experiment proved problematic, as the precise sphere packing density was unknown. That work, however, demonstrated the potential of a Monte Carlo model of the XPCi microbubble signal,[16] which we developed here for polydisperse microbubbles of clinically relevant radii and concentration, both for three-image retrieval and single-shot approaches. This model was put together using the McXtrace software package as a framework.[17]

To simulate the passage of a photon through the sample, first each bubble is tested (in order of distance from the source) to find whether it is hit by the current photon. In that case, an intersection point is calculated, and the photon propagated to this point. Absorption by the medium the photon has passed through to reach the bubble is accounted for by adjusting the photon weight according to the Beer-Lambert law. A refraction angle is then calculated in 3D using Snell's law, and the photon direction changed accordingly. The bubble is tested again to determine whether the photon passes through or is deflected from the bubble surface; if it passes through, refraction is calculated again. Absorption within the bubble can also be included (as for the medium), but is not strictly necessary due to the low attenuation of the filling gas. This process is repeated until the photon exits the sample. The container walls are also simulated, again using the Beer-Lambert law with the appropriate thickness and refractive index input into the simulation.

Refraction at a microbubble boundary is calculated using Eqs. 1-3, where n_1 is the refractive index of the medium, n_2 is the refractive index of the bubble filling gas, $\mathbf{i}$ is the normalised vector describing the incident photon, $\mathbf{r}$ is the normalised vector of the refracted photon, and $\mathbf{n}$ is the normal to the surface of the sphere. θ_i is the incident angle and θ_r is the refracted angle, both relative to the normal to the sphere's surface.

$$\mathbf{r} = \frac{n_1}{n_2}\mathbf{i} - \left(\frac{n_1}{n_2}\cos\theta_i + \sqrt{1-\sin^2\theta_r}\right)\mathbf{n} \qquad (1)$$

$$\sin^2\theta_r = \left(\frac{n_1}{n_2}\right)^2 \times (1-\cos^2\theta_i) \qquad (2)$$

$$\cos\theta_i = \mathbf{i}\cdot\mathbf{n} \qquad (3)$$

At the analyzer crystal, the vector describing the photon propagation is resolved into two angles: θ on the x-z plane and ϕ on the z-y plane. The angle θ is used as input to the function describing the analyzer crystal reflectivity, as the analyzer crystal is primarily sensitive to angular deviations on the x-z plane. For simulating images taken on the maximum and half maximum positions of the RC, fitting with a single Gaussian is sufficient, as around these positions a Gaussian closely fits the experimental RC. However, the tails of the RCs are not well reproduced. Hence, for simulating images taken on the RC tail, the experimental RC was interpolated using a cubic method, and a finely sampled version of this interpolation used in the simulation to describe the crystal response. This approach removes the problem of fitting an analytical function to the RC, thus increasing the comparability between simulation and experiment.

Sphere arrangement was performed using code written by the authors, which works as follows. Spheres are placed in a random position within the volume, and checked for overlap after each addition. Spheres are added until the required concentration is reached. To arrange polydisperse spheres, each is positioned randomly in descending size order; this allows reaching higher concentrations more efficiently. In fact, this method is efficient enough to allow for sphere arrangements to be generated for each simulation run, with all simulation work shown here performed using a single standard desktop computer (Intel i7-2600s 2.8GHz), which indicates high potential for future expansion of the simulation framework.

For both simulation and experiment, scatter and apparent absorption retrieval were performed using the generalized diffraction enhanced imaging (GDEI) equations.[7] GDEI was used as it allows for scatter retrieval using only three images whilst also taking into account the position of the crystal for each image.

The crystal reflectivity was measured by calculating the ratio between the readings of two ion chambers (ICs) placed either side of the crystal. Practical limitations mean that the crystal reflectivity can be known more accurately than it is possible to position the crystal. When processing experimental images, GDEI equations were therefore applied using the recorded crystal reflectivity and closest RC in time.

The first problem to overcome when attempting quantitative work with microbubbles is that they float, so a method is needed to keep the suspension homogeneous; the second is that microbubbles typically burst. Lack of control of these two factors mean that the size distribution and concentration cannot be accurately determined.

To overcome the first problem, microbubbles were held in a viscous suspension. The solution was made by diluting ultrasound coupling gel until the point at which the microbubbles started to float, then slightly increasing the gel proportion. This mixture was vacuum pumped to remove any air bubbles before a known quantity of microbubbles was gently stirred into the gel, without break-

ing the surface to prevent the introduction of additional air bubbles. The gel mixture was imaged alongside water to check for any refractive index difference, and none was found.

This method for sample preparation has the advantage that no temperature change is required, reducing the risk of damage to the microbubbles. Three different sample thicknesses were imaged, with a depth in the direction of x-ray propagation of 10.0 mm, 4.1 mm and 0.68 mm. All container walls were made of PMMA with 1 mm, 1 mm and 0.68 mm thickness respectively.

To overcome bubble bursting, Expancel microbubbles (Casco Products AB, Sundsvall, Sweden) were used, as they have a rigid co-polymer outer shell making them very stable.[18] They also have both a size distribution (median radius 4.5 μm) and filling gas refractive index comparable to clinically used microbubbles.

Microbubble concentration and size distribution were calculated using the method described by Sennoga et al,[19] and these values were used as input for the simulation and data analysis, thus enabling simulation of the samples imaged experimentally. Microbubble concentration is here defined as fraction by volume, with all concentrations chosen within a range used clinically.

The experiment was carried out at the SYRMEP beamline of the ELETTRA synchrotron facility (Trieste, Italy), using an energy of 17 KeV selected by a Si(1 1 1) double-crystal monochromator, with third harmonic components being insignificant due to the use of a bending magnet and relatively low electron energy in the storage ring. The analyzer crystal placed between the sample and detector was a double bounce analyzer obtained with two single flat Si(1 1 1) crystals. Samples were scanned using a high resolution CCD camera (Photonic Science, Robertsbridge, UK) with a 9 μm pixel size. Each sample was imaged with the crystal positioned as accurately as possible at the RC maximum and the two symmetric half-slope positions, as well as on the tail at nominal 2.5% of peak reflectivity. The actual crystal reflectivity (given by the ratio of the ICs) was recorded for each image for use in the analysis. Flat field images were taken for every sample image, and rocking curves and detector dark current images were acquired at regular intervals.

All simulations were carried out using a 64 by 64 pixel array with the size as used experimentally, with 2×10^7 photons used to simulate each experimental image.

For simulation of the full three-image GDEI processing, the crystal reflectivity was fixed to be at precisely the two half maximums and maximum of the RC, with a RC full width at half maximum (FWHM) equal to the average of all experimental RCs measured (18.1 μrad). When processing the experimental data, GDEI equations were applied using the precise crystal reflectivity measured by the ICs and the RC measurement taken at the closest time; however the variability among the measured RCs was minimal.

As can be seen from Fig. 2, a good match was found for the extracted absorption signal between simulation and experiment using three different container depths. Increasing bubble concentration is shown to slightly decrease the apparent absorption signal. This is because larger scatter distribution widths, associated with higher bubble concentrations, result in extinction effects that reduce the apparent absorption signal.[7]

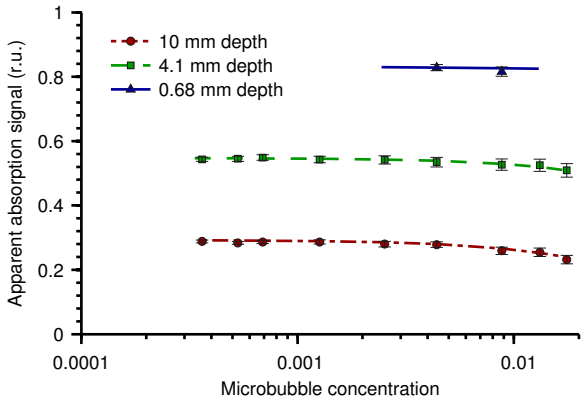

FIG. 2. Extracted apparent absorption signal as a function of microbubble concentration for simulation (lines) and experiment (dots), for three depths of container.

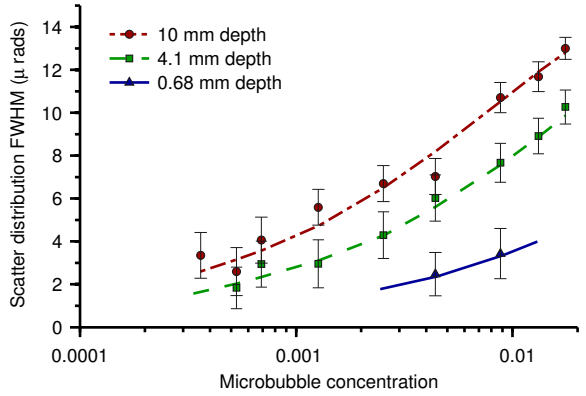

FIG. 3. Scatter signal extracted through the GDEI algorithm as a function of microbubble concentration for simulation (lines) and experiment (dots), for three depths of container.

Figure 3 shows the comparison of simulation and experiment for the FWHM of the scatter distribution extracted using the GDEI algorithm. A very close fit can be seen for the 0.68 mm and 4.1 mm deep container, as well as the 10 mm deep container at higher concentrations. Increasing both microbubble concentration and sample thickness results in a wider scatter distribution. The variability of recorded signal for the thicker sample at lower microbubble concentrations can be explained by the much higher sample absorption decreasing the detected flux.

Finally, we report on proof-of-concept quantitative agreement (for the 4.1 mm thick sample) for a single-shot method which would be essential for *in-vivo* implemen-

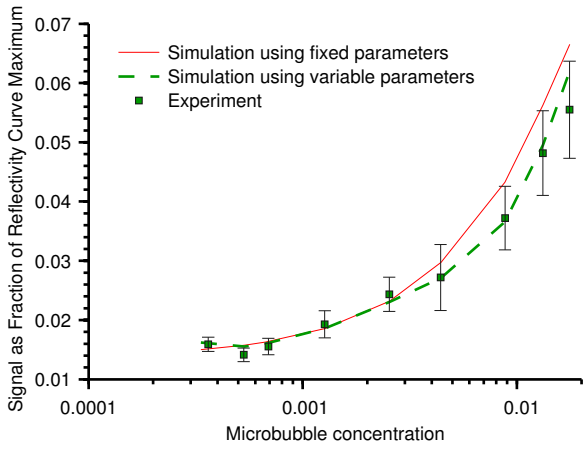

FIG. 4. Comparison between simulation and experimental results for single-shot scatter imaging on the RC tail. Simulation for fixed RC parameters (red line) and variable RC parameters from the experiments (green dashed line) are shown, with the experimental data represented by green squares.

tations and could open the way to dynamic imaging.

Figure 4 shows the results of two simulations obtained by interpolating experimental RCs in different ways. For the red line, the RC measured for the first point was used to simulate all concentrations, with crystal reflectivity fixed at 0.025. For the green line, the closest RC in time and precise crystal reflectivity for each sample was used, leading to much better agreement. This is because signal on the tail of the RC derives from sample scatter, RC shape, and in a small part sample absorption, and has a strong dependence on the crystal reflectivity. Despite efforts to keep the equipment consistent between measurements, some change could not be avoided. The practical implication of this is that, if the system is not sufficiently stable, to enable effective quantitation of microbubble concentration the reflectivity of the analyzer crystal must be monitored during imaging. This could be done for example by using a small region of the radiation field not covered by the sample.

This work has presented the experimental validation of a quantitative Monte Carlo model for simulating microbubble imaging using ABI. In addition to providing the basis for using the Monte Carlo model for more complex geometries (e.g. phantoms containing variable microbubble concentrations) and 3D studies, this enables quantification of microbubble concentrations from scatter images of a sample (including single-shot), for example by fitting data series generated 'ad hoc' by the model. This can enable both functional implementations of x-ray imaging (e.g. perfusion studies), and assessment of targeted drug delivery - for example if microbubbles filled with a specific drug are burst in a specific location by means of a highly focused ultrasound beam.

Alongside the relevance to *in-vivo* synchrotron studies, e.g. on small animals or even on humans along the lines of the mammography work currently underway at ELETTRA,[20] in the longer term this could be applicable to compact systems, and consequently transferable into a clinical environment. Examples are the quoted work on Talbot/Lau methods,[6,13–15] or our own lab-based edge illumination method,[21] for which a geometrical optics approach has already been demonstrated,[22] and proven to give practically the same results as the more rigorous wave-optics approach when an incoherent laboratory source is used.[23] Validation of the Monte Carlo model using ABI now gives a solid basis for translating the microbubble simulation to this laboratory based system.

ACKNOWLEDGMENTS

This work is funded by EPSRC (Grants EP/G004250/1, EP/I021795 and EP/I021884/1).

[1] A. Snigirev, I. Snigireva, V. Kohn, S. Kuznetsov, and I. Schelokov, Rev. Sci. Instrum. **66**, 5486 (1995).
[2] S. W. Wilkins, T. E. Gureyev, D. Gao, A. Pogany, and A. W. Stevenson, Nature **384**, 335 (1996).
[3] T. J. Davis, D. Gao, T. E. Gureyev, A. W. Stevenson, and S. W. Wilkins, Nature **373**, 595 (1995).
[4] L. Rigon, H.-J. Besch, F. Arfelli, R.-H. Menk, G. Heitner, and H. Plothow-Besch, J. Phys. D: Appl. Phys. **36**, A107 (2003).
[5] E. Pagot, P. Cloetens, S. Fiedler, A. Bravin, P. Coan, J. Baruchel, J. Hartwig, and W. Thomlinson, Appl. Phys. Lett. **82**, 3421 (2003).
[6] F. Pfeiffer, M. Bech, O. Bunk, P. Kraft, E. F. Eikenberry, C. Bronnimann, C. Grunzweig, and C. David, Nat Mater **7**, 134 (2008).
[7] L. Rigon, F. Arfelli, and R.-H. Menk, Appl. Phys. Lett. **90**, 114102 (2007).
[8] F. Arfelli, L. Rigon, and R. H. Menk, Phys. Med. Biol. **55**, 1643 (2010).
[9] R. Tang, Y. Xi, W.-M. Chai, Y. Wang, Y. Guan, G.-Y. Yang, H. Xie, and K.-M. Chen, Phys. Med. Biol. **56**, 3503 (2011).
[10] A. Velroyen, M. Bech, A. Malecki, A. Tapfer, A. Yaroshenko, M. Ingrisch, C. C. Cyran, S. D. Auweter, K. Nikolaou, M. Reiser, and F. Pfeiffer, Phys. Med. Biol. **58**, N37 (2013).
[11] J. G. Brankov, M. N. Wernick, Y. Yang, J. Li, C. Muehleman, Z. Zhong, and M. A. Anastasio, Medical Physics **33**, 278 (2006).
[12] Y. Nesterets, Optics Communications **281**, 533 (2008).
[13] W. Yashiro, Y. Terui, K. Kawabata, and A. Momose, Opt. Express **18**, 16890 (2010).
[14] S. K. Lynch, V. Pai, J. Auxier, A. F. Stein, E. E. Bennett, C. K. Kemble, X. Xiao, W.-K. Lee, N. Y. Morgan, and H. H. Wen, Appl. Opt. **50**, 4310 (2011).
[15] A. Malecki, G. Potdevin, and F. Pfeiffer, EPL (Europhysics Letters) **99**, 48001 (2012).
[16] A. Khromova, F. Arfelli, H. Besch, H. Plothow-Besch, R. Menk, and L. Rigon, in *IEEE Nuclear Science Symposium Conference Record*, Vol. 6 (2004) pp. 4014–4018 Vol. 6.
[17] E. Bergbäck Knudsen, A. Prodi, J. Baltser, M. Thomsen, P. Kjær Willendrup, M. Sanchez del Rio, C. Ferrero, E. Farhi, K. Haldrup, A. Vickery, R. Feidenhans'l, K. Mortensen, M. Meedom Nielsen, H. Friis Poulsen, S. Schmidt, and K. Lefmann, Journal of Applied Crystallography **46**, 679 (2013).
[18] E. Stride and N. Saffari, Ultrasonics, Ferroelectrics and Frequency Control, IEEE Transactions on **52**, 2332 (2005).
[19] C. A. Sennoga, V. Mahue, J. Loughran, J. Casey, J. M. Seddon, M. Tang, and R. J. Eckersley, Ultrasound in Medicine & Biology **36**, 2093 (2010).
[20] E. Castelli, M. Tonutti, F. Arfelli, R. Longo, E. Quaia, L. Rigon, D. Sanabor, F. Zanconati, D. Dreossi, A. Abrami, E. Quai, P. Bregant, K. Casarin, V. Chenda, R. H. Menk, T. Rokvic,

A. Vascotto, G. Tromba, and M. A. Cova, Radiology **259**, 684 (2011).
[21] A. Olivo and R. Speller, Appl. Phys. Lett. **91**, 074106 (2007).
[22] A. Olivo and R. Speller, Phys. Med. Biol. **52**, 6555 (2007).
[23] P. R. Munro, K. Ignatyev, R. D. Speller, and A. Olivo, Opt. Express **18**, 4103 (2010).